Coherent radiation of relativistic nonlinear Thomson scattering

K. Lee
Laboratory for Quantum Optics, Korea Atomic Energy Research Institute, P. O. Box 105, Deokjin-Dong, Yuseong, Daejeon 305-600, Korea

B. H. Kim and D. Kim
Physics Department, Pohang University of Science and Technology, San 31 Hyoja-Dong, Nam Ku, Pohang, Kyungbuk 790-784, Korea

(Received 23 February 2004; accepted 31 January 2005; published online 25 March 2005)

The condition for the coherent addition of the relativistic nonlinear Thomson scattered (RNTS) radiations from a group of electrons is derived. Numerical calculations show that under such a condition, all the characteristics of RNTS radiation by a single electron are maintained, leading to the generation of intense attosecond x rays. Such an attosecond x ray is produced in a specific direction with a very narrow angular divergence. An x-ray radiation of $\sim 10^{16}$ W/cm^2 with a pulse width of 7.7 as is expected for an oblique irradiation of a 20 fs linearly polarized laser pulse of 4×10^{19} W/cm^2 on a 7 nm thick film target. For the proof-of-principle experiment, the radiation characteristics from a 50 nm thick film target are presented and discussed. © *2005 American Institute of Physics*. [DOI: 10.1063/1.1878832]

I. INTRODUCTION

Relativistic plasma, a new regime in physics, has been opened due to the development in ultraintense laser technology during the past decade.[1,2] Not only the fundamental aspect of relativistic plasma are attractive but also its potential application seems to be significant especially in the area of the generation of high energy particles such as electrons, ions, positrons, and γ rays.[3] The generation of x-ray radiation with a pulse width of subfemtoseconds presently draws much attention because such a radiation allows one to explore ultrafast dynamics of electrons and nucleons.

Several schemes have been proposed and/or demonstrated to generate an ultrashort x-ray pulse: the relativistic Doppler shift of a backscattered laser pulse by a relativistic electron beam,[4–6] the harmonic frequency upshift of a laser pulse by relativistic nonlinear motion of electrons,[6–17] high order harmonic generation in the interaction of intense laser pulse with noble gases[18–21] and solids,[22–27] and x-ray laser using inner shell atomic transitions.[28,29] The train of a few 100 as pulses has been observed in the case of laser-noble gas interaction.[19–21]

When a low-intensity laser pulse is irradiated on an electron, the electron undergoes a harmonic oscillatory motion and generates a dipole radiation with the same frequency as the incident laser pulse, which is called Thomson scattering.[30] As the laser intensity increases, the oscillatory motion of the electron becomes relativistically nonlinear, which leads to the generation of harmonic radiations, referred to as relativistic nonlinear Thomson scattered (RNTS) radiation. The motion of the electron begins to be relativistic as the following normalized vector potential approaches to unity:

$$a_o = 8.5 \times 10^{-10} \lambda I^{1/2}, \tag{1}$$

where λ is the laser wavelength in μm and I the laser intensity in W/cm^2.

The RNTS radiation has been investigated in analytical ways.[6–13] Recently, indebted to the development of the ultraintense laser pulse, experiments on RNTS radiation have been carried out by irradiating a laser pulse of 10^{18}–10^{20} W/cm^2 on gas jet targets.[14–17] A numerical study in the case of single electron has been attempted to characterize the RNTS radiation[12] and a subsequent study has shown that it has a potential to generate a few attosecond x-ray pulse.[13] Even a scheme for the generation of a zeptosecond x-ray pulse using two counter propagating circularly polarized laser pulses has been proposed.[11]

The main properties[17] which make RNTS radiation different from Bremsstrahlung radiation are known to be (1) incoherent radiation or, linear dependence of the radiation intensity on an electron density, (2) broad and peaked spectrum, and (3) strongly anisotropic angular distribution. However to maintain the ultrashort characteristics of RNTS by a single electron, all the scattered radiations from a plasma should be coherently superposed, that is, the radiation intensity should increase quadratically on electron density. This motivation has led us to a condition for a coherent superposition of RNTS radiations from a plasma. The numerical simulations on this condition have been conducted and revealed that for an ultrathin target, the characteristics of the RNTS radiation by single electron is indeed preserved at a specified direction and the RNTS radiation energy might exceed Bremsstrahlung radiation energy.

II. A CONDITION FOR COHERENT RNTS

To maintain the ultrashort pulse width or wide harmonic spectrum of a single electron radiation even in the case of a group of electrons, it is required that the radiations from different electrons should be coherently added at a detector. In the case of RNTS radiation, which contains many harmonic wavelengths, such a requirement can be satisfied only if all the differences in the optical paths of the radiations

from electrons to a detector be almost zero. The above condition can be practically restated: all the time intervals that scattered radiations from different electrons take to a detector should be comparable with or less than the attosecond pulse width of a single electron radiation.

Scattered radiations by individual electrons are calculated using the relativistic Newton's equation of motion and the formula for the radiation field by a moving charged particle,[12] and then all the scattered radiation fields from a plasma should be evaluated at a detector. An analytic approach for this is hardly possible. However, the time intervals that radiations take to a detector can be readily obtained with the following assumptions as the first-order approximation: (1) plane wave of a laser field, (2) no Coulomb interaction between charged particles, thus neglecting ions, and (3) neglect of initial thermal velocity distribution of electrons during the laser pulse.

The quivering amplitude of an electron is about 0.6 μm for the laser intensity of 4×10^{19} W/cm^2. Considering a typical focal size of a laser pulse as 10 μm, the transverse variation of a laser intensity can then be neglected during the motion of each electron. But the transverse intensity variation of a laser pulse could affect the total scattered radiation from electrons at different transverse positions, which will be discussed at the end of Sec. III. For a 20 fs FWHM (full width at half maximum) pulse width with a laser intensity of 4×10^{19} W/cm^2, an electron propagates about 20 μm in the direction of the laser propagation during the laser pulse, which is comparable to a typical depth of focus of about 10 μm. The inclusion of the paraxial propagation of the laser pulse would make electrons feel more rapid decrease of the laser field during the long longitudinal motion due to the defocusing of the laser pulse. Thus the plane wave approximation might affect the intensity of the scattered radiation by a small factor but the main characteristics of the radiation would be maintained.

With respect to Coulomb interaction between charged particles, a critical density has been estimated, below which the influence of ion field on electrons could be neglected.[12] For a finite thickness target, the mean free path would be a good parameter to estimate the effect of ion fields. Using the electron-ion collisional time,[31] in which the velocity of electrons driven by the laser pulse is used instead of a thermal velocity, for an electron density of 10^{22} cm^{-3}, the mean free path ranges from 10 μm to 10 cm for the electron velocity $0.1c$–c, where c is the speed of light. This justifies the neglect of Coulomb interaction for the target thickness of submicrometers.

Without any prepulse, the target material would be ionized through optical field ionization in the rising phase of an ultrashort laser pulse, thus producing a plasma. Considering this as an initial state of the plasma, the thermal temperature might be in the order of a few eV which is negligibly small compared with the kinetic energies of relativistic electrons driven by the intense part of the laser field during which RNTS radiation is emitted. Hence the neglect of thermal distribution of electrons or the frozen electron model (electrons initially at rest) is justified.

With these assumptions, a plasma is modeled as a group of electrons without ions. The radiation field by the ith electron, $\vec{f}_i(t)$ at an initial position of $\vec{r}_i=(x_i,y_i,z_i)$, due to irradiation of an ultraintense laser pulse propagating $+z$ direction can be calculated from that of an electron initially at origin and just considering the time intervals between the electrons Δt_i,

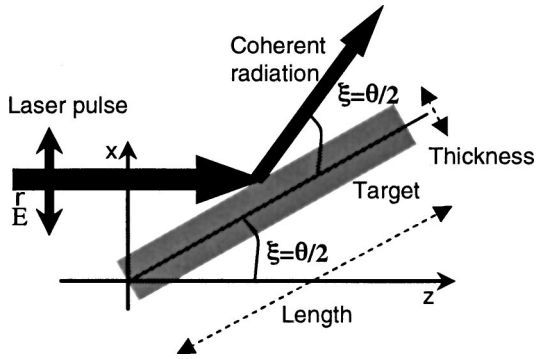

FIG. 1. Schematic diagram of the target and the laser pulse for the coherent RNTS radiation.

$$\Delta t_i = \Delta t_i' - \frac{\hat{n}\cdot\vec{r}}{c}, \tag{2}$$

where $\Delta t_i' = z_i/c$ is the time which the laser pulse takes to arrive at the ith electron from origin and $\hat{n}$ the unit vector of the radiation direction: $\vec{f}_i(t)=\vec{f}_o(t-\Delta t_i)$, where $\vec{f}_o(t)$ is the radiation field from an electron initially at origin which is calculated by the formulas described in Ref. 12. Then all the radiation fields from different electrons are summed on a detector to obtain a total radiation field, $\vec{F}(t)$ as

$$\vec{F}(t) = \sum_i \vec{f}_o(t-\Delta t_i). \tag{3}$$

The condition for a coherent superposition in x-z plane can now be formulated by setting Eq. (2) to be less or equal to the pulse width of single electron radiation Δt_{FWHM}^s as follows (see Fig. 1):

$$|z\tan\xi - x| \leqslant \frac{c\Delta t_{FWHM}^s}{\sin(2\xi)}, \tag{4}$$

where $\xi=\theta/2$. For a polar angle ϕ, $\phi=0°$ is inserted into Eq. (2), because the maximum harmonic radiation appears at this direction in the case of a linearly polarized laser pulse and is symmetric in the case of a circularly polarized one. Equation (4) manifests that RNTS radiations are coherently added to the specular direction of an incident laser pulse off the target, if the target thickness, T is restricted to

$$T \leqslant \frac{c\Delta t_{FWHM}^s}{\sin\xi}. \tag{5}$$

Since the incident angle of the laser pulse can be set arbitrarily, one can set θ to the direction of the maximum radiation of a single electron, θ_M. For a linearly polarized laser of 4×10^{19} W/cm^2 and 20 fs FWHM, the calculation in the case of a single electron (Fig. 2) shows that $\Delta t_{FWHM}^s=5$ as, and $\theta_M=27°$. Equation (5) then indicates that the target

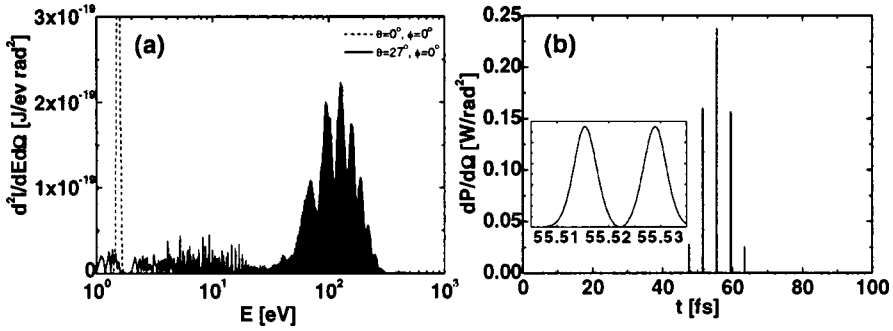

FIG. 2. RNTS by a single electron for a linearly polarized laser pulse of 4×10^{19} W/cm^2 and 20 fs FWHM. (a) Angular harmonic spectrum and (b) angular power at the direction of $\theta=27°$ and $\phi=0°$. The inset of (b) shows the enlarged central double peaks. It is shown that the radiation contains energy spectrum from a few tens to 200 eV with a pulse width of 5 as FWHM.

thickness should be less than 7 nm. This target thickness is hardly realized in near future. However to an extent, the above restriction in thickness can be relaxed to demonstrate a coherent RNTS radiation. A proof-of-principle experiment with a commercially available 50 nm thick film target is proposed at the end of Sec. III to demonstrate our coherent condition for RNTS radiation.

III. NUMERICAL CALCULATIONS AND DISCUSSIONS

For the demonstration of the derived condition for the coherent RNTS radiation, numerical simulations have been conducted with the assumptions presented in the preceding section. For a laser pulse, the parameters of a typical Ti:sapphire laser having a Gaussian temporal shape were adopted: 800 nm for wavelength, 4×10^{19} W/cm^2 ($a_o=4.3$) for intensity and 20 fs FWHM for pulse width with the laser propagating along the z direction and the electric field of the laser pulse being at the x direction (Fig. 1).

The features of the scattered radiations of two different configurations of target were compared: (A) oblique incidence on an ultrathin target of 7 nm in thickness, 5 μm in width, 20 μm in length, 10^{16} cm^{-3} in electron density, and $\xi=13.5°$ and (B) normal incidence on the base of a thick cylindrical target of 1 μm in thickness and radius, and 10^{18} cm^{-3} in electron density. The electron densities of 10^{16} and 10^{18} cm^{-3} used here were chosen for the convenience of the calculation because as will be discussed later, it is found that the density (or the total number of electrons) affects only the intensity of the scattered radiation, but not its harmonic spectral and temporal shape. The condition (A) corresponds to the condition for coherent RNTS radiation [Eq. (4)], while the condition (B) can be considered similar to the recent experimental condition with gas target[17] in the sense of its incoherent radiation as will be seen later. The calculated harmonic spectrum and power to a direction of $\theta=27°$ and $\phi=0°$ are plotted in Fig. 3 for the conditions (A) and (B). The direction is the specular direction of the incident laser pulse in the case of condition (A). For the coherent target configuration [condition (A)], one can find that the harmonic spectrum and power [Figs. 3(a) and 3(b)] have almost the same structure as those from a single-electron radiation [Figs. 2(a) and 2(b)] in terms of high-energy photon spectrum and ultrashort pulse width. As expected from the analysis in the preceding section, the shorter delays between radiations from different electrons than the pulse width of single-electron radiation makes the radiations superposed coherently reproducing the radiation by a single electron except for much increased intensity. On the other hand, in the case of the condition (B), the radiation characteristics [Figs. 3(c) and 3(d)] are completely different due to an incoherent summa-

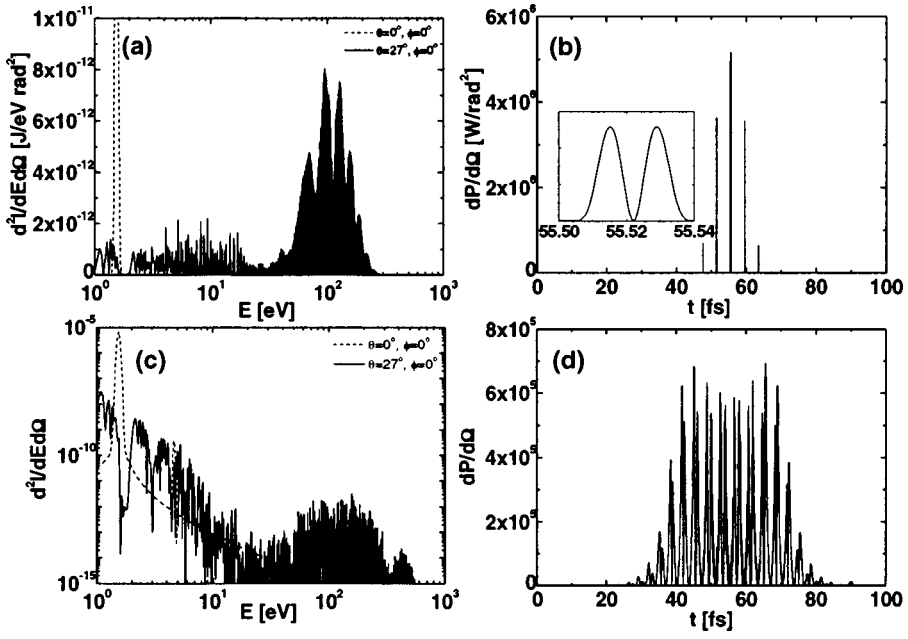

FIG. 3. RNTS for two different target conditions described in the text as condition (A) and (B). (a) and (b) are angular harmonic spectra and angular power for condition (A) at $\theta=27°$ and $\phi=0°$, respectively, and (c) and (d) for condition (B). (a) and (b) shows almost the same structure as Figs. 2(a) and 2(b). The enlarged central double peaks in the inset of (b) show 7.7 as FWHM. The spectrum to $\theta=0°$ direction is shown in (a) and (c) for comparison. The intensity of the fundamental radiation in (a) is as large as 3×10^{-11} J/(eV rad^2).

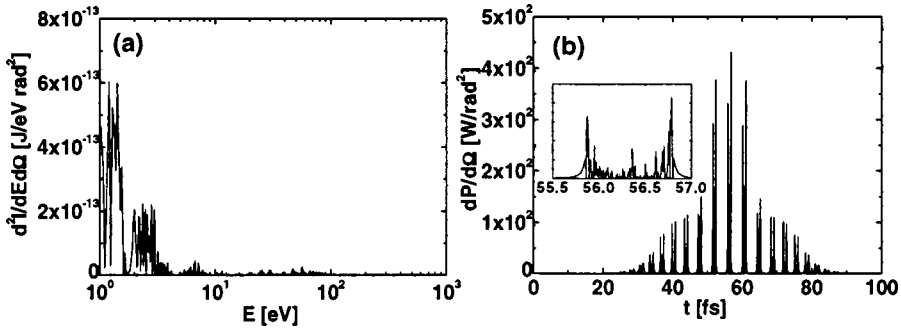

FIG. 4. (a) Angular harmonic spectrum and (b) angular power at the direction $\theta=30°$ and $\phi=0°$, which are completely different from those for the condition (*A*) in Figs. 3(a) and 3(b) in terms of spectral, power shape, and intensity.

tion of the radiations, which will be analyzed later. In the spectrum by a single electron, the intensity at 100 eV region is much higher but for a normal irradiation on a thick cylinder target, the intensities of low-energy photons increase more than those of high-energy photons. Especially, the maximum intensity of the fundamental radiation is seven orders of magnitude larger than those of the harmonic radiations, while for the case of the condition (*A*), the maximum intensity of the fundamental radiation is only four times higher than those of harmonic radiations. The comparison of the temporal shapes of the radiations at the direction of $\theta=27°$ and $\phi=0°$ shows that there is no attosecond pulse for the condition (*B*). It should be mentioned that with a single electron and a thin target, the direction of the radiation peak is $\theta=27°$ and $\phi=0°$ but with a thick cylinder target, the radiation peak appears at $\theta=0°$, because the dipole or fundamental radiation becomes most intense.

Since the coherent superposition condition is matched at a specified direction, the radiation to a slightly different direction, e.g., $\theta=30°$, shows completely different characteristics as shown in Figs. 4(a) and 4(b): stronger in low-energy spectrum, power reduction by four orders of magnitude, and complicated pulse shape. This direction-matching condition for the coherent superposition leads to a very narrow angular divergence. This property would be useful in an actual application since the spatial selection of the most intense part of the radiation would guarantee an attosecond pulse, which is difficult to measure in a time domain.

These numerical results described in the above well demonstrate the condition for the coherent RNTS radiation derived in the previous section. For a circularly polarized laser pulse, similar calculations have been conducted, which showed the same results as those for a linearly polarized laser pulse.

The dependence of the pulse width on target thickness has been analyzed considering the temporal profile of the radiation field by a single electron. In the case of a linearly polarized laser pulse, one component of the radiation field from a single electron, $f(t)$ is plotted in Fig. 5, in which the inset shows the enlarged central peak. The total field from a uniformly distributed electrons, $F(t)$ can be obtained by integrating $f(t)$ over the volume as

$$F(t) = \rho \int f(t,\vec{r}) d^3\vec{r}, \tag{6}$$

where ρ is the number density of the electron. The usage of the relations between electrons [Eq. (2)], with a change of variable in Eq. (6), leads to the following equation:

$$F(t) = \frac{N}{T}\int_{t-Q/2}^{t+Q/2} f(\eta) d\eta, \tag{7}$$

where N is the total number of electrons in the volume, T the target thickness, and $Q=2T\sin\xi/c$. Considering the properties of the field function in the inset of Fig. 5 such as odd symmetry and larger peak-to-peak interval (t^s_{pp}) than the width of each peak (Δt^s_{FWHM}), Δt_{FWHM} (the pulse width of $|F(t)|^2$) can be approximately obtained for two extreme cases:

$$\Delta t_{FWHM} \simeq \begin{cases} Q & \text{for } Q \ll \Delta t^s_{FWHM} \\ t^s_{pp} - \Delta t^s_{FWHM} & \text{for } Q \gg t^s_{pp}. \end{cases} \tag{8}$$

This indicates that the pulse width increases with thickness and then becomes saturated. The increase of the pulse width on the target thickness can be easily understood considering the superposition of the peaks radiated from different electrons with slight shift in time. The saturation of the pulse width in the case of a linearly polarized laser pulse is caused by the double peaks having opposite phases. As the thickness increases more, the radiation peaks having opposite phases among different electrons begin to be destructively interfered causing the pulse width saturated. However in the case of a circularly polarized laser pulse, due to the single peak nature the pulse width keeps increasing as the thickness increases. This has been also manifested in numerical simulations whose results are shown in Fig. 6. Figure 6 shows the dependence of pulse width on target thickness for a linearly [Fig. 6(a)] and a circularly [Fig. 6(b)] polarized laser in the specular direction of the incident laser pulse. The simulation results in Fig. 6 are obtained for different thicknesses at a

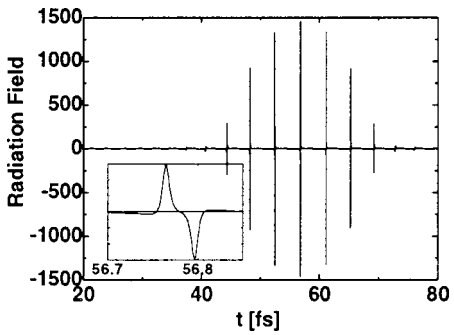

FIG. 5. The *x* component of the radiation field toward $\theta=30°$ and $\phi=0°$ for Fig. 2.

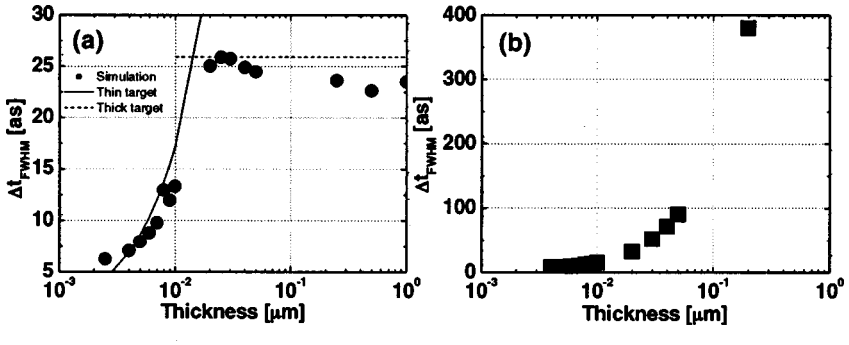

FIG. 6. The dependence of a pulse width on target thickness is plotted for different laser polarization: (a) linear and (b) circular. The data are obtained for the target parameters: electron density, 10^{15} cm^{-3}; width, 5 μm; length, 10 μm. The ξ's are 15° (θ=30° and ϕ=0°) and 17° (θ=34° and ϕ=0°) for the linear and the circular polarization, respectively. The approximated pulse widths in extreme cases of ultrathin and thick target thickness [Eq. (8)] are also plotted in (a).

given target parameters of 10^{15} cm^{-3} for electron density, 5 μm for target width, and 10 μm for target length. The laser pulses irradiate a target with ξ=15° and ξ=17° for the linear and the circular polarization, respectively. For a linearly polarized laser, the pulse width indeed increases with thickness and becomes saturated at large thicknesses [Fig. 6(a)]. However, for a thick target, another complication sets in due to the interference between adjacent peaks. This interference strongly alters the pulse shape. For a circularly polarized laser pulse, the single peak nature,[12] or even symmetry of the field profile makes the pulse width keep increasing as the target thickness increases as shown in Fig. 6(b). A series of simulations has been performed also for different electron densities, target thicknesses, and target lengths. The results reveal that while the thickness dramatically varies the pulse width or shape, other target parameters such as width, length, and density do not affect the pulse shape.

The degree of coherence is analyzed by introducing the following enhancement factor α defined as

$$P_N^* = P_1^* N^\alpha, \tag{9}$$

where P_N^* and P_1^* are the peak radiation power from a plasma with N electrons and from a single electron, respectively. The dependence of the enhancement factor on target thickness for a linear polarization is plotted in Fig. 7(a) for the same target parameters (open circles) as Fig. 6(a). One can notice that as the target gets thinner, α approaches 2, meaning that the radiation becomes coherent. On the contrary, as the target gets thicker, it becomes incoherent as observed in recent experiments.[16,17] The enhancement factor not only depends on the target thickness and but also on the other target parameters. To understand this behavior, the enhancement factor is analyzed using Eq. (7). Rewriting Eq. (9) for α with the help of Eq. (7) yields

$$\alpha = 2 - \frac{B}{\log N}. \tag{10}$$

Now the coefficient B depends only on the thickness as

$$B = 2 \ln\left(Q \frac{f^*}{G^*} \right), \tag{11}$$

where G is the integral in Eq. (7) without N/T. The superscript, * for each variable indicates its peak value in time. Equation (10) shows the weak dependence of the enhancement factor on the total number of electrons N as shown in Fig. 7(a). The symbols other than the open circle in Fig. 7(a) represent the simulation results for the different total number of electrons but with the same thickness. On the other hand, as plotted in Fig. 7(b), the coefficient B depends only on the target thickness for the same condition as in Fig. 7(a). This coefficient, once obtained, is very useful to estimate the intensities of the radiation for different densities or target sizes without an actual simulation. This provides the justification that the simulation at reduced densities would be still useful for the understanding in the case of high densities as was in Fig. 2.

The dependence of the angular structure of scattered radiations on target thickness and length are plotted in Figs. 8(a) and 8(b), respectively. For a better comparison, each line is normalized to its peak. As the thickness increases, the

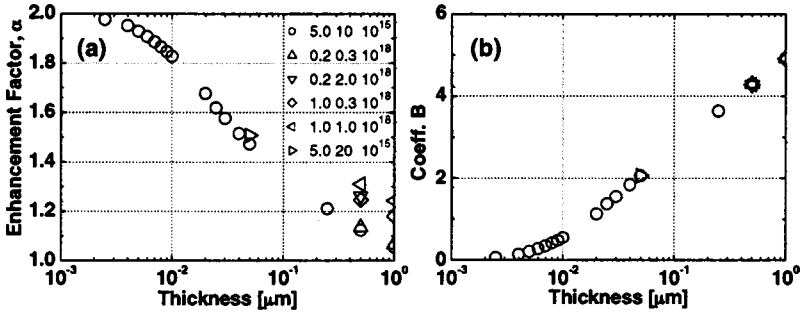

FIG. 7. (a) The enhancement factor α and (b) coefficient B defined by Eqs. (10) and (11), respectively, are plotted in the case of a linearly polarized laser. The parameters shown in the legend of (a) represent width (μm), length (μm), and electron density (cm^{-3}) in order for each symbol. The target parameters for open circles are the same as in Fig. 6(a). It is noticed that while the enhancement factor depends not only on thickness but also on the total number of electrons, the coefficient B depends only on target thickness.

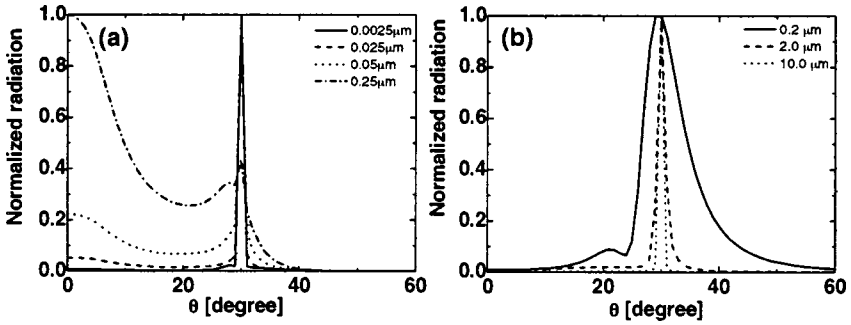

FIG. 8. The dependence of the angular distributions on (a) target thickness and (b) target length is plotted for an electron density of 10^{15} cm^{-3}, a width of 5 μm, and $\xi=15°$. The length for (a) is fixed at 10 μm and the thickness for (b) at 2.5 nm.

fundamental radiation is enhanced much more than high-order harmonics, which makes the radiation at $\theta=0°$ more intense [Fig. 8(a)]. As the length increases, more radiators within a volume make the radiation enhanced more in that direction and the angular width narrower as shown in Fig. 8(b). However the structures of the harmonic spectrum and the power at the matched direction are not affected. These angular characteristics are much different from the recent experimental data with a helium gas target irradiated by 7×10^{19} W/cm^2 intensity laser.[17] Our calculational results suggest that their observation may include significant contributions from other physical processes.

From the simulation results for the condition (*A*), the peak intensity of the radiation 10 cm away from the source is estimated to be $\sim10^{16}$ W/cm^2 taking the angular divergence of 0.1° and a solid density of 10^{22} cm^{-3}. The total energy of the RNTS radiation is also estimated to be more than 100 μJ. With a laser energy of 260 mJ, 60% of which being within a focal spot of 5 μm in diameter, the conversion efficiency of the laser energy to all the high-order harmonic radiation is estimated to be more than 4×10^{-4}. This conversion efficiency is a few hundred times higher than that in the case of high harmonic generation with Xe gas[18] and glass target.[27]

RNTS radiation is emitted during the interaction of a laser pulse with electrons and Bremsstrahlung radiation begins to be significant afterwards. Even though two different radiations are separated in time, it is difficult to distinguish them in real experimental situations. Thus in order for RNTS radiation to be measured with a certainty, Bremsstrahlung radiation should be negligible compared with RNTS radiation. The total energy of Bremsstrahlung radiation for the case of this study is estimated to be about 0.1 μJ according to the formula described in Ref. 31 for an electron temperature of 100 eV, an electron density of 10^{22} cm^{-3} and a duration of 10 ns. This is significantly smaller than the estimated energy of RNTS radiation. Considering the long collision length of an electron under such an intense laser pulse, the majority of electrons might escape the target without any collision with ions and Bremsstrahlung radiation might be then even weaker than estimated. The experimental geometry suggested in this study will lead to a clean observation of RNTS radiation.

The extreme condition for a target thickness such as 7 nm makes the demonstration of such an ultrashort pulse hardly possible in the near future. Even though the 7 nm thickness of a target is critical to achieve a few attosecond x-ray pulse, such a restriction can be relaxed to an extent that subfemtosecond radiations in a few 10 eV range can be generated. Thus the authors propose a proof-of-principle experiment with a film target of 50 nm thickness, which is commercially available. The calculated harmonic spectrum and angular distributions are plotted in Figs. 9(a) and 9(b), respectively. The pulse width is estimated to be 20 as or so [Fig. 6(a)], which is still attractive as an attosecond radiation source. The estimated energy of the RNTS radiation is about 60 μJ, which still exceeds the Bremsstrahlung radiation of a few microjoules. Hence the modulated harmonic spectrum and the sharp angular distribution are expected to be measured. Since the thickness is a very important factor in this analysis, to prevent the plasma from being expanded much before a main pulse, a very high contrast ratio in 1 ps (10^{10} or higher) of an ultraintense drive laser is required.[32,33]

It is important to address the effect of the nonuniform intensity distribution of a laser pulse in a focal area on the phases of the scattered radiations. The coherent condition [Eq. (4)] is derived by comparing the pulse width of single electron's radiation, Δt^s_{FWHM} with delay in the arrivals of the radiations from different electrons. The delay is determined by geometrical factors but the pulse width of a single electron's radiation has been found to be scaled on the laser

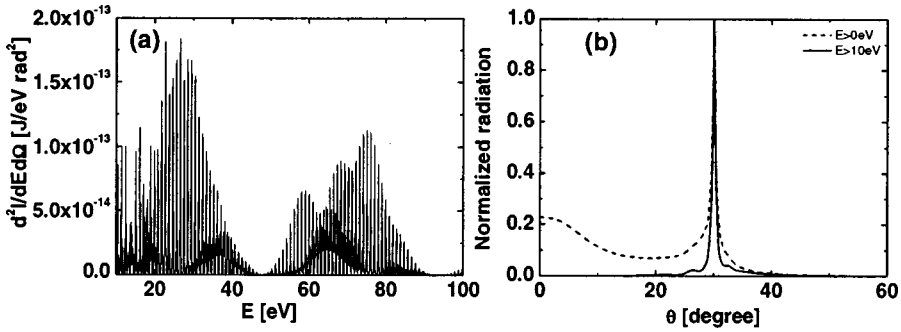

FIG. 9. For a target thickness of 50 nm (a) angular harmonic spectrum and (b) angular power at $\theta=30°$ and $\phi=0°$ are plotted for 10^{15} cm^{-3} in electron density, 5 μm in target width, 10 μm in target length, and $\xi=15°$. In (b), the dotted line is the intensity integrated over the whole spectrum and the solid line over the spectrum larger than 10 eV.

intensity I as $\Delta t^s_{FWHM} \propto I^{-1.4}$.[13] This leads to the following relation between the variations of a laser intensity and pulse width:

$$\frac{\delta(\Delta t^s_{FWHM})}{\Delta t^s_{FWHM}} = 1.4\frac{\delta I}{I}, \tag{12}$$

where δ indicates the variation. Then within a FWHM focal area, $\delta I/I = 0.5$, the pulse width of each electron's radiation varies up to 70%. Moreover the angular power of the scattered radiation varies on the laser intensity to the power of 4.7.[13] Thus radiations by the electrons out of a focal area or a coherent region can be neglected, leaving the total RNTS radiation coherent. This steep dependence of the radiation power on the laser intensity could reduce the total radiation power, which is estimated to be less than in the case of uniform laser intensity by a factor of 3 around.

Another important factor to be considered is plasma dynamics including the propagation of a laser pulse through an overdense plasma, especially in the case of the 50 nm thick target experiment. The relativistic critical plasma density is calculated to be 1.7×10^{22} cm^{-3}, which is close to the plasma density of 10^{22} cm^{-3} used in the estimation of the radiation energy. The relativistic skin depth of 170 nm is rather longer than the target thickness. The hole-boring problem could be considered by estimating the speed of ion front.[34,35] In the case of the shorter pulse width than a potential sweeping time of $\sim$80 fs,[35] the ion velocity is estimated to be $\sim 7\times10^7$ cm/s for fully ionized titanium, of which a film target is available with a thickness of 50 nm. Then the traveling distance of ions during the laser pulse is $\approx$14 nm, which is much shorter than the propagation distance of electrons, say about 20 μm and even shorter than the target thickness. This estimation shows that the ion propagation due to holeboring could be neglected in the current analysis. Recent numerical simulation by Dong *et al.*[36] shows that if the plasma thickness is comparable with or less than the skin depth, an ultraintense laser pulse can propagate with a few 10% absorption and little reflection even through an overdense plasma, for example, 100 times denser than the critical plasma density. Even though the numerical study did not include a holeboring problem, the results show that our current analysis up to a few 10 nm plasma thickness with a density of 10^{22} cm^{-3} could be applicable. However, to estimate the radiation intensity and the pulse width more accurately, the dynamics of an ultrathin film irradiated by an ultraintense laser pulse and the radiations from individual electrons need to be treated at the same time.

IV. SUMMARY

A condition for coherent superposition to get an intense attosecond x-ray through RNTS radiation has been derived and numerically demonstrated. It is shown that when an ultraintense laser pulse of 4×10^{19} W/cm^2 and 20 fs FWHM is irradiated on an ultrathin target of 7 nm at an incident angle of 76.5° from a target normal, an intense x-ray radiation of $\sim10^{16}$ W/cm^2 with 7.7 attosecond FWHM in the range of 100 eV could be generated. The total energy by the RNTS radiation (100 μJ) is estimated to exceed the Bremsstrahlung radiation (0.1 μJ) by three orders of magnitude, which makes it possible to detect the RNTS radiation without a time-resolved experiment.

The conversion efficiency from an optical laser to harmonic radiations is also estimated to be 4×10^{-4}, which is much higher than the other harmonic generation schemes. It should be pointed that the geometrical condition for the coherent RNTS radiation is very similar to the moving plasma mirror model,[26] even though that the physical mechanisms are completely different.

The derived condition and the calculational results show that RNTS radiation with a normal film or a gas target does not produce attosecond pulse and makes the fundamental (dipole) radiation prevail over high-order harmonic radiations.

A proof-of-principle experiment is proposed with a relaxed target condition: a target thickness of 50 nm. It is still expected in this situation that the RNTS is highly angular and stronger than Bremsstrahlung.

ACKNOWLEDGMENTS

Without the linux-cluster system supported by Dr. H. K. Joo at Korea Atomic Energy Research Institute, the numerical data might not be obtained.

This work was supported by the Korean Research Foundation Grant (Grant No. KRF-2000-015-DP0175) and by the Brain Korea 21 project in 2003.

[1] M. D. Perry and G. Mourou, Science **264**, 917 (1994).
[2] G. A. Mourou, C. P. J. Barty, and M. D. Perry, Phys. Today **51**, 22 (1998).
[3] D. Umstadter, J. Phys. D **36**, R151 (2003).
[4] P. Sprangle, A. Ting, E. Esarey, and A. Fisher, J. Appl. Phys. **72**, 5032 (1992).
[5] F. V. Hartemann, Phys. Plasmas **5**, 2037 (1998).
[6] E. Esarey, S. K. Ride, and P. Sprangle, Phys. Rev. E **48**, 3003 (1993).
[7] Vachaspati, Phys. Rev. **128**, 664 (1962).
[8] L. S. Brown and T. W. B. Kibble, Phys. Rev. **133**, A705 (1964).
[9] E. Esarey and P. Sprangle, Phys. Rev. A **45**, 5872 (1992).
[10] Y. Ueshima, Y. Kishimoto, A. Sasaki, and T. Tajima, Laser Part. Beams **17**, 45 (1999).
[11] A. E. Kaplan and P. L. Shkolnikov, Phys. Rev. Lett. **88**, 074801 (2002).
[12] K. Lee, Y. H. Cha, M. S. Shin, B. H. Kim, and D. Kim, Opt. Express **11**, 309 (2003).
[13] K. Lee, Y. H. Cha, M. S. Shin, B. H. Kim, and D. Kim, Phys. Rev. E **67**, 026502 (2003).
[14] S.-Y. Chen, A. Maksimchuk, and D. Umstadter, Nature (London) **396**, 653 (1998).
[15] S.-Y. Chen, A. Maksimchuk, E. Esarey, and D. Umstadter, Phys. Rev. Lett. **84**, 5528 (2000).
[16] S. Banerjee, A. R. Valenzuela, R. C. Shah, A. Maksimchuk, and D. Umstadter, Phys. Plasmas **9**, 2393 (2002).
[17] K. Ta Phuoc, A. Rousse, M. Pittman, J. P. Rousseau, V. Malka, S. Fritzler, D, Umstadter, and D. Hulin, Phys. Rev. Lett. **91**, 195001 (2003).
[18] A. L'Huillier and Ph. Balcou, Phys. Rev. Lett. **70**, 774 (1998).
[19] P. M. Paul, E. S. Toma, P. Breger, G. Mullot, F. Auge, Ph. Balcou, H. G. Muller, and P. Agostini, Science **292**, 1689 (2001).
[20] E. Hertz, N. A. Papadogiannis, G. Nersisyan, C. Kalpouzos, T. Halfmann, D. Charalambidis, and G. D. Tsakiris, Phys. Rev. A **64**, 051801 (2001).
[21] M. Hentschel, R. Kienberger, Ch. Spielmann, G. A. Reider, N. Milosevic, T. Brabec, P. Corkum, U. Heinzmann, M. Drescher, and F. Krausz, Nature (London) **414**, 509 (2001).
[22] D. von der Linde, T. Engers, G. Jenke, P. Agostini, G. Grillon, E. Nibbering, A. Mysyrowicz, and A. Antonetti, Phys. Rev. A **52**, R25 (1995).
[23] P. A. Norreys, M. Zepf, S. Moustaizis, A. P. Fews, J. Zhang, P. Lee, M. Bakarezos, C. N. Danson, A. Dyson, P. Gibbon, P. Loukakos, D. Neely, F. N. Walsh, J. S. Wark, and A. E. Dangor, Phys. Rev. Lett. **76**, 1832 (1996).

[24]R. Lichters, J. Meyer-ter-Vehn, and A. Pukhov, Phys. Plasmas **3**, 3425 (1996).
[25]D. von der Linde and K. Rzazewski, Appl. Phys. B: Lasers Opt. **63**, 499 (1996).
[26]D. von der Linde, Appl. Phys. B: Lasers Opt. **68**, 315 (1999).
[27]A. Tarasevitch, A. Orisch, D. von der Linde, Ph. Balcou, G. Rey, J.-P. Chambaret, U. Teubner, D. Klopfel, and W. Theobald, Phys. Rev. A **62**, 023816 (2000).
[28]D.-E. Kim, C. Toth, and C. P. J. Barty, Phys. Rev. A **59**, R4129 (1999).
[29]D. Kim, S. H. Son, J. H. Kim, C. Toth, and C. P. J. Barty, Phys. Rev. A **63**, 023806 (2001).
[30]J. Sheffield, *Plasma Scattering of Electromagnetic Radiation* (Academic, New York, 1975).
[31]Lyman Spitzer, *Physics of Fully Ionized Gases*, 2nd ed. (Wiley, New York, 1962).
[32]B. Dromey, S. Kar, M. Zepf, and P. Foster, Rev. Mod. Inst. **75**, 645 (2004).
[33]G. Doumy, F. Quere, O. Gobert, M. Perdrix, Ph. Martin, P. Audebert, J. C. Gauthier, J.-P. Geindre, and T. Wittmann, Phys. Rev. E **69**, 026402 (2004).
[34]S. C. Wilks, W. L. Kruer, M. Tabak, and A. B. Langdon, Phys. Rev. Lett. **69**, 1383 (1992).
[35]Y. Sentoku, T. E. Cowan, A. Kemp, and H. Ruhl, Phys. Plasmas **10**, 2009 (2003).
[36]Q. L. Dong, Z.-M. Sheng, M. Y. Yu, and J. Zhang, Phys. Rev. E **68**, 026408 (2003).